0026-895X/07/7204-907–920$20.00
MOLECULAR PHARMACOLOGY
Copyright © 2007 The American Society for Pharmacology and Experimental Therapeutics
Mol Pharmacol 72:907–920, 2007

Vol. 72, No. 4
37333/3254757
Printed in U.S.A.

Subunit-Specific Agonist Activity at NR2A-, NR2B-, NR2C-, and NR2D-Containing *N*-Methyl-D-aspartate Glutamate Receptors

Kevin Erreger, Matthew T. Geballe, Anders Kristensen, Philip E. Chen, Kasper B. Hansen, C. Justin Lee, Hongjie Yuan, Phuong Le, Polina N. Lyuboslavsky, Nicola Micale, Lars Jørgensen, Rasmus P. Clausen, David J. A. Wyllie, James P. Snyder, and Stephen F. Traynelis

Department of Pharmacology, Emory University School of Medicine, Rollins Research Center, Atlanta, Georgia (K.E., A.K., K.B.H., C.J.L., H.Y., P.L., P.N.L., S.F.T.); Department of Chemistry, Emory University, Atlanta, Georgia (M.T.G., J.P.S.); Centre for Neuroscience Research, University of Edinburgh, Hugh Robson Building, George Square, Edinburgh, United Kingdom (P.E.C., D.J.A.W.); and Department of Medicinal Chemistry, Faculty of Pharmaceutical Sciences, University of Copenhagen, Copenhagen, Denmark (N.M., L.J., R.P.C.).

Received April 22, 2007; accepted July 10, 2007

ABSTRACT

The four *N*-methyl-D-aspartate (NMDA) receptor NR2 subunits (NR2A-D) have different developmental, anatomical, and functional profiles that allow them to serve different roles in normal and neuropathological situations. Identification of subunit-selective NMDA receptor agonists, antagonists, or modulators could prove to be both valuable pharmacological tools as well as potential new therapeutic agents. We evaluated the potency and efficacy of a wide range of glutamate-like compounds at NR1/NR2A, NR1/NR2B, NR1/NR2C, and NR1/NR2D receptors. Twenty-five of 53 compounds examined exhibited agonist activity at the glutamate binding site of NMDA receptors. Concentration-response relationships were determined for these agonists at each NR2 subunit. We find consistently higher potency at the NR2D subunit for a wide range of dissimilar structures, with (2*S*,4*R*)-4-methylglutamate (SYM2081) showing the greatest differential potency between NR2A- and NR2D-containing receptors (46-fold). Analysis of chimeric NR2A/D receptors suggests that enhanced agonist potency for NR2D is controlled by residues in both of the domains (Domain1 and Domain2) that compose the bilobed agonist binding domain. Molecular dynamics (MD) simulations comparing a crystallography-based hydrated NR1/NR2A model with a homology-based NR1/NR2D hydrated model of the agonist binding domains suggest that glutamate exhibits a different binding mode in NR2D compared with NR2A that accommodates a 4-methyl substitution in SYM2081. Mutagenesis of functionally divergent residues supports the conclusions drawn based on the modeling studies. Despite high homology and conserved atomic contact residues within the agonist binding pocket of NR2A and NR2D, glutamate adopts a different binding orientation that could be exploited for the development of subunit selective agonists and competitive antagonists.

NMDA receptors are ligand-gated ion channels that mediate a component of excitatory synaptic transmission that can trigger changes in synaptic strength (Malenka and Nicoll, 1993). NMDA receptors have also been implicated in the pathophysiology of stroke and brain injury (Wang and Shuaib, 2005), epilepsy (Mares et al., 2004), as well as a range of psychiatric disorders (Heresco-Levy and Javitt, 1998; MacDonald and Chafee, 2006). NMDA receptors are tetrameric protein complexes composed of a combination of glycine-binding NR1 subunits and glutamate-binding NR2 subunits (Dingledine et al., 1999; Chen and Wyllie, 2006). The subunit arrangement is probably a dimer of two NR1/

This work was supported by National Institutes of Health grant NS36654 (to S.F.T.), the Michael J. Fox Foundation (to S.F.T.), the National Alliance for Research on Schizophrenia and Depression (to S.F.T.), the Alfred Benzon Foundation (to A.S.K., K.B.H.), the Howard Hughes Medical Institute (to K.E.), and Biotechnology and Biological Sciences Research Council grant BB/D001978/1 (to D.J.A.W.).

Article, publication date, and citation information can be found at http://molpharm.aspetjournals.org.

doi:10.1124/mol.107.037333.

ABBREVIATIONS: NMDA, *N*-methyl-D-aspartate; MD, molecular dynamics; *cis*-ACPD, (1*R*,3*R*)-aminocyclopentane-*cis*-1,3-dicarboxylate; *trans*-ACPD, (1*R*,3*S*)-aminocyclopentane-*trans*-1,3-dicarboxylic acid;; L-CCG-IV, (2*S*,3*R*,4*S*)-2-(carboxycyclopropyl) glycine; L-CCG-I, (2*S*,3S,4*S*)-2-(carboxycyclopropyl) glycine; MTSEA, methanethiosulfonate ethylammonium; *cis*-ADA, *cis*-azetidine-2,4-dicarboxylic acid; SYM2081, (2*S*,4*R*)-4-methylglutamate; ANOVA, analysis of variance; ACBD, 1-aminocyclobutane-1,3-dicarboxylic acid; RMSD, root-mean-square deviation.

NR2 heterodimers (Furukawa et al., 2005). Four different NR2 subunits (NR2A-D) have been identified with distinct expression and functional profiles (Erreger et al., 2004). This heterogeneity among NMDA receptor subunits creates an opportunity to identify subunit selective agonists, partial agonists, antagonists, and modulators. Among these, most success has been achieved with the development of NR2B selective antagonists, which have received significant attention as potential therapeutic candidates (Chazot, 2004; Borza and Domany, 2006; Layton et al., 2006).

Although the pharmacology of the glutamate binding site of NMDA receptors has been examined in native preparations (Patneau and Mayer, 1990; Benveniste and Mayer, 1991; Curras and Dingledine, 1992; Jane et al., 1994) as well as in *Xenopus laevis* oocytes injected with whole-brain RNA (Verdoorn and Dingledine, 1988), no systematic or complete analysis exists that investigates structure-activity relationships for NMDA glutamate-site agonists acting at all individual NR2 subunits. To better understand structural features of subunit selectivity of agonists for this class of receptors, we have compared the effect of a wide range of glutamate-like compounds at recombinant heterodimeric NMDA receptors.

We used two-electrode voltage-clamp recordings of *X. laevis* oocytes coexpressing the NR1 subunit together with the NR2A, NR2B, NR2C, or NR2D subunit to characterize the agonist properties of the glutamate-like compounds. We examined chimeric NR2A-NR2D receptors to determine the structural basis for differences in agonist activity between NR2D and NR2A subunits. We subsequently used molecular dynamics (MD) simulations to compare a homology model of the agonist binding domain complex for NR1/NR2D to a recently released crystal structure of the agonist binding domain complex of NR1/NR2A (Furukawa et al., 2005). From the structural analyses, we have developed a working hypothesis about differential agonist binding principles in NR2A compared with NR2D. The ideas were tested by functionally evaluating a complementary set of point mutants made at analogous residues within the NR2A and NR2D binding domains. The diverse methods provide insight into the structural features of the agonist-binding site that determine agonist structure-activity profiles at NMDA receptor NR2 subunits.

Materials and Methods

Electrophysiology. cRNA for rat NR1–1a (hereafter NR1) and NR2A, -B, -C, and -D were synthesized in vitro and injected (5–10 ng) into *X. laevis* oocytes isolated as described previously (Traynelis et al., 1998). Rat cDNAs for NR1 and NR2 subunits [GenBank accession numbers: NR1, U11418 and U08261; NR2A, D13211; NR2B, U11419; NR2C, M91563; NR2D, L31611 (modified according to Monyer et al., 1994)] were provided by Drs. S. Heinemann (Salk Institute), S. Nakanishi (Kyoto University), and P. Seeburg (University of Heidelberg). Two-electrode voltage-clamp current recordings were made 24 to 72 h after injection. The recording solution contained (in) 90 mM NaCl, 3 mM KCl, 10 mM HEPES, 0.5 mM $BaCl_2$, 0.01 mM EDTA, 0.05 mM glycine (23°C); pH was adjusted to 7.3 with NaOH. EDTA (10 μM) was added to chelate contaminant extracellular divalent ions, including trace amounts of Zn^{2+}. Solution exchange was computer controlled through an eight-modular-valve positioner (Digital MVP Valve; Hamilton Company, Reno, NV). Voltage and current electrodes were filled with 0.3 and 3.0 M KCl, respectively, and current responses recorded at a holding potential of −40 mV. Data acquisition and voltage control were accomplished with a two-electrode voltage-clamp amplifier (OC-725; Warner Instruments, Hamden, CT). Responses of the wild-type receptors to agonists were expressed as a percentage of the mean response to 100 μM ($\geq$20× EC_{50}) glutamate applied at the beginning and end of each protocol. Most glutamate analogs were purchased from Tocris (Ellisville, MO) with the following exceptions: *N*-methyl-L-aspartate, L-glutamate, L-homocysteinesulfinate, D-homocysteinesulfinate, L-homocysteate, D-homocysteate, L-cysteinesulfinate, L-cysteate, and L-CCG-IV were purchased form Sigma (St. Louis, MO); L-aminoadipic acid, D-aminoadipic acid, *trans*-ACPD, and (1*R*,3*R*)-homo-ACPD were purchased from Alexis (Lausen, Switzerland); phenylglycine-*o*-carboxylic acid was purchased from MP Biomedicals (Irvine, CA); 4-fluoro-glutamate was purchased from Apollo Scientific (Bredbury, UK); and methanethiosulfonate ethylammonium (MTSEA) was purchased from Toronto Research Chemicals Inc. (Toronto, Canada). The racemic mixture of 2-(*N*-hydroxypyrazol-4-yl)glycine was synthesized as described previously (Cali and Begtrup, 2002; Clausen et al., 2004) and enantiomers separated with a CR(+) Crownpak column (150 × 10 mm) using 0.1% aqueous trifluoroacetic acid as eluent. D-Cysteic acid was prepared from D-cysteine as described previously (Darkwa et al., 1998). Recordings from at least six oocytes from two different frogs were performed for all active compounds. Data were pooled among oocytes and composite dose-response data were fitted by the equation Percentage Response = 100 × Relative Efficacy/[1 + (EC_{50}/Concentration)^{n_H}], where EC_{50} is the concentration of agonist that produces a half-maximal response, Relative Efficacy is the response at maximally effective concentration relative to the maximal response of glutamate, and n_H is the Hill slope. All parameters were allowed to vary during the fitting procedure, with the exception of Relative Efficacy for NR1/NR2A *cis*-ADA, which was fixed to 100% because of low potency; we were unable to obtain enough *cis*-ADA to test concentrations higher than 3 mM.

Mutagenesis and Expression of Chimeric NR2A/NR2D Plasmid Constructs. The oocyte expression plasmids containing the rat NR2A or NR2D NMDA subunit cDNAs have been described previously; residue numbering of the mature polypeptides started at the predicted cleavage site for the signal peptide (Chen et al., 2004, 2005). The NR2A/2D chimeras were generated using polymerase chain reaction-based strategies. The necessary NR2D region was amplified using *Pfu* turbo (Stratagene, La Jolla, CA) with primers that incorporated the flanking NR2A subcloning sites. Chimeric NR2A/D subunits were generated by replacing Val370 to Val518 in the NR2A subunit with Leu385 to Val539 from the NR2D subunit [referred to as the NR2A(2D-S1) chimera] and by replacing Glu638 to Ilel795 in the NR2A subunit with Glu659 to Ile812 from the NR2D subunit [referred to as the NR2A(2D-S2) chimera]. All chimeras were confirmed by DNA sequencing. Site-directed mutagenesis was performed using the QuikChange mutagenesis kit (Stratagene). For in vitro cRNA synthesis, cDNAs were linearized with NotI or MluI and run-off transcripts were synthesized using T7 or SP6 polymerase based kits according to manufacturers' protocols (Promega, Madison, WI, or Ambion, Austin, TX).

Molecular Modeling. Starting from the crystal structure of the NR1/NR2A agonist binding domain dimer (Protein Data Bank code 2A5T), a model of the NR1/NR2D agonist binding domain dimer was constructed using the comparative modeling package in Prime (Schrödinger, Portland, OR). The agonist binding domains of NR2A and NR2D show 72% sequence identity and 82% homology in the alignment. The sequence of NR2A in our model was also modified to represent the wild-type polypeptide, which involved removal of a short linker peptide and addition of two unresolved residues in the crystal structure 2A5T. The NR1/NR2D interface was subjected to multiple rounds of side chain optimization and energy minimization using Prime to alleviate any strain introduced by homology modeling. Analysis with PROCHECK (Laskowski et al., 1993) reveals little difference in the overall G factor between the crystal structure (0.34)

and the NR1/NR2D homology model (0.21); scores above −0.5 are considered acceptable. The glycine and glutamate ligands were left in their crystallographic positions before unrestrained molecular dynamics simulation in which both protein and ligand can move. Structures with SYM2081 in the NR2 binding site used the crystallographic glutamate ligand as the basis for initial SYM2081 placement. These complexes were then prepared for molecular dynamics (MD) simulation using GROMACS v. 3.2.1 (Berendsen et al., 1995; Lindahl et al., 2001). Ligand and protein were treated using the GROMOS96 force field, and then solvated with 26,500 water molecules (SPC water model) and five or six chloride ions to neutralize overall charge. After a 50-ps simulation with ligand and protein restrained to allow for water equilibration, a 10-ps simulation was performed at 50 K to remove any gross steric clashes from the structures. The simulation was then restarted at 50 K and the temperature was increased to 300 K over 250 ps. These simulations were continued at 300 K for 10 ns (SYM2081 complexes were simulated for 5 ns). All simulations were performed with NPT conditions (constant number of particle, pressure, and temperature) using the Berendsen thermostat (Berendsen et al., 1984) and a particle mesh Ewald electrostatics treatment (Essman et al., 1995) with a cutoff of 9 Å. The 10-ps simulation at 50 K used a time step of 1 fs; all other simulations used a 2-fs time step. Average structures were prepared from the final 2 ns of simulation. All figures from MD simulations were produced using VMD (Humphrey et al., 1996). Analysis using Hingefind (Wriggers and Schulten, 1997) was performed on the average structures. Partitioning with ε of 2.5 resulted in two domains that were most similar to D1 and D2 in composition. Additional hinge measurements were performed by manually selecting D1 and D2 as the two rigid domains.

Alignment of cyclic glutamate analogs and SYM2081 to the crystallographic glutamate ligand was performed using ROCS (v. 2.2; OpenEye Scientific Software, Inc., Santa Fe, NM), after a conformational search by OMEGA (v. 2.0; OpenEye Scientific Software). Default parameters were used for OMEGA, and scoring with color was used for analysis by Rapid Overlay of Chemical Structures (ROCS). Figures of the alignment were produced using VIDA (v 2.1.1, OpenEye Scientific Software).

Results

Subunit Preferences of NMDA Receptor Glutamate-Like Compounds. A series of 52 compounds were evaluated for agonist activity at recombinant NR1/NR2A, NR1/NR2B, NR1/NR2C, or NR1/NR2D NMDA receptors at a test concentration of 100 μM. At this concentration, compounds producing less than 20% of the current response to glutamate at all subunit combinations were not investigated further (28 compounds; Fig. 1). All other active compounds were tested on a

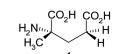
1

(2*S*)-alpha-methylglutamate (N=5-8)

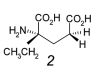
2

(2*S*)-alpha-ethylglutamate (N=6-8)

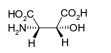
3

L-threo-3-hydroxyaspartate (N=6-8)

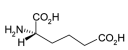
4

L-aminoadipic acid (N=6)

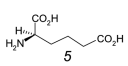
5

D-aminoadipic acid (N=6)

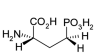
6

D-2-amino-4-phosphonobutyric acid (N=6-8) (D-AP4)

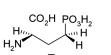
7

L-2-amino-4-phosphonobutyric acid (N=8) (L-AP4)

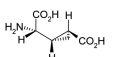
8

(2*S*,3S,4*S*)-2-(carboxycyclopropyl) glycine (N=6-8) (L-CCG-I)

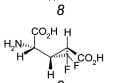
9

(2*S*,3*S*,4*S*)-2-(2'-carboxy-3,3'-difluorocyclopropyl)glycine (N=6-8)

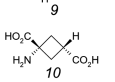
10

cis-1-aminocyclobutane-1,3-dicarboxylic acid (N=7-8) (cis-ACBD)

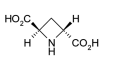
11

trans-azetidine-2,4-dicarboxylic acid (N=6-8) (*trans*-ADA)

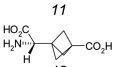
12

(*S*)-(+)2(3'carboxybicyclo[1.1.1]pentyl)glycine (N=6) ((*S*)-(+)-CBPG)


13

(2*R*,4*R*)-4-aminopyrrolidine-2,4-dicarboxylic acid (2*R*,4*R*-APDC) (N=6-8)

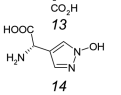
14

(*S*)-NHP4G (N=7-9)


15

(1*R*,3*R*)-homo-ACPD (N=6-7)

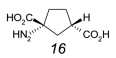
16

(1*R*,3*S*)-aminocyclopentane-*trans*-1,3-dicarboxylic acid (*trans*-ACPD) (N=6)

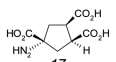
17

(1*S*,3*R*,4*S*)-1-aminocyclopentane-1,3,4-tricarboxylic acid (ACPT-I) (N=7-9)

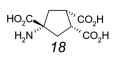
18

(1*R*,3*R*,4*S*)-1-aminocyclopentane-*trans*-1,3,4-tricarboxylic acid (ACPT-II) (N=6-8)

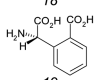
19

phenylglycine-o-carboxylic acid (N=6-8)

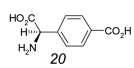
20

(*R*)-4-carboxyphenylglycine (N=6-8)

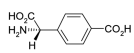
21

(*S*)-4-carboxyphenylglycine (N=6-12)

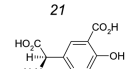
22

(*R*)-3-carboxy-4-hydroxyphenylglycine (N=6)

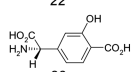
23

(*S*)-3-carboxy-4-hydroxyphenylglycine (N=6)

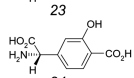
24

(*S*)-4-carboxy-3-hydroxyphenylglycine (N=6)

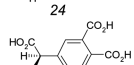
25

(*R*)-3,4-dicarboxyphenylglycine (DCPG) (N=6)

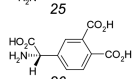
26

(*S*)-3,4-dicarboxyphenylglycine (DCPG) (N=6)

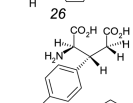
27

(2*R*,3*S*)-chlorophenylglutamate (N=6-8)

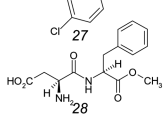
28

N-L-alpha-aspartyl-L-phenylalanine 1-methyl ester (Aspartame) (N=6)

Fig. 1. A list of inactive glutamate-like compounds evaluated at 100 μM (plus 50 μM glycine) at recombinant NR1/NR2A, NR1/NR2B, NR1/NR2C, and NR1/NR2D receptors in *X. laevis* oocytes is shown. Compounds producing <20% of the current relative to 100 μM glutamate at all subunit combinations were not studied further. The number of oocytes tested at each NR1/NR2 subunit combination is provided in parentheses.

minimum of six oocytes for each subunit combination, which included recordings from oocytes from at least two different frogs.

Compounds exhibiting agonist activity were further studied to determine the concentration-response relationship for each agonist at each NR1/NR2 subunit combination. The standard recording protocol and current response is illustrated in Fig. 2 for a representative compound, L-homocysteate (compound 40). Increasing concentrations of the test compound were applied and the current response was normalized to the mean of the maximal glutamate response at the beginning and end of each recording (Fig. 2A). Oocytes that showed marked rundown (>25%) of the glutamate response at the end of the experiment compared with the initial response were discarded. Normalized data were pooled among oocytes for each subunit combination and the composite concentration-response curve was generated (Fig. 2B). The concentration-response relationship was fitted with the logistic equation (see *Materials and Methods*) to determine the EC_{50} and relative efficacy for each agonist at the four NR2 subunits. In this study, the term relative efficacy is used to describe the current response to a saturating concentration of the agonist relative to the maximal current response to glutamate. Although this assigns glutamate a relative efficacy of 1.0, we recognize that absolute glutamate efficacy defined by open probability is considerably lower than 1.0 for some receptors (Wyllie et al., 1998; Erreger et al., 2004). Furthermore, we use the term potency to refer to EC_{50}, high potency indicating low EC_{50} values and low potency indicating high EC_{50} values. The fitted EC_{50} values, Hill slopes, and relative efficacy are summarized in Figs. 3 to 5 for all active compounds. Although potency is often influenced by agonist efficacy (Colquhoun, 1998; see below), there is no significant correlation between agonist potency and efficacy either within an individual subunit or across all subunits ($p > 0.05$ for all; Student's t test); correlation coefficients were $r = 0.043$ (NR2A), $r = -0.051$ (NR2B), $r = -0.11$ (NR2C), $r = 0.17$ (NR2D), and $r = 0.046$ (all subunits). For all compounds, there was no significant difference in relative agonist efficacy among NR1/NR2A, NR1/NR2B, NR1/NR2C, and NR1/NR2D receptors ($p = 0.18$, one-factor ANOVA). There was no clear trend relating efficacy and potency across the compounds we studied. In addition, with the exception of 2-(*N*-hydroxypyrazol-4-yl)glycine (52; numbers in parentheses throughout the text refer to the compound numbers in the structure columns in Figs. 1 and 3 to 5), most agonists had relative efficacies, compared with glutamate, between 0.5 and 1.0; virtually all of the dicarboxylic acids or other agonists studied were highly efficacious. This may reflect structural conservation of functionality across our set of test compounds, because all but three of the compounds are aspartate or glutamate analogs and contain at least one strongly acidic proton from either CO_2H, SO_2H, or SO_3H.

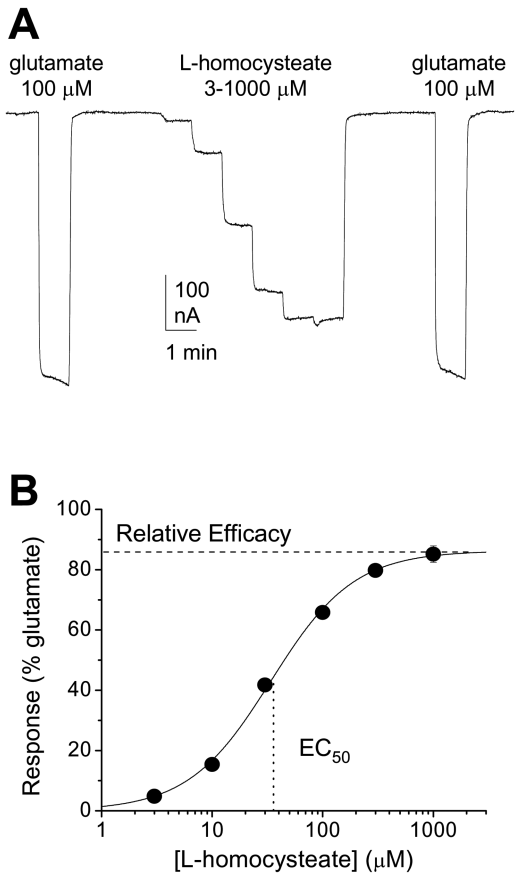

Fig. 2. A, a representative two-electrode voltage-clamp current recording illustrating the standard protocol and response for analysis of the concentration-response curve. An oocyte expressing NR1/NR2A was exposed to maximally effective concentrations of glutamate plus glycine, followed by increasing concentrations of the test compound plus glycine, and finally glutamate and glycine again. Currents were normalized to the mean of the two glutamate responses. B, the corresponding average composite concentration-response curve is shown (L-homocysteate for NR1/NR2A; $n = 13$). Error bars are S.E.M. and are shown when larger than symbol size. The current responses are normalized to the maximal response to glutamate.

Homocysteate and cysteinesulfinate acid have long been known to be agonists at the NMDA receptor (Mayer and Westbrook, 1987; Curras and Dingledine, 1992). L-Homocysteate (40) and L-cysteinesulfinate (42) are taken up by CNS tissue (Grieve et al., 1992). Moreover, sulfur-containing amino acids are released from brain in a Ca^{2+}-dependent fashion, suggesting they could serve as neurotransmitters (Do et al., 1986, 1988). Their ability to initiate NMDA receptor-dependent cell death has led to further speculation that they may be endogenous excitotoxins (e.g., Lehmann et al., 1993). Figure 4 summarizes the response of a series of D and L sulfur-containing glutamate and aspartate analogs, which were active at all NR2 subunits in the low to high micromolar range. The rank order of potency was similar to glutamate, with compounds being most potent at NR2D-containing receptors and least potent at NR2A-containing receptors. Of the various compounds studied, L-homocysteate (40) and D-homocysteinsulfinate (39) were most potent, activating NR1/NR2D NMDA receptors with an EC_{50} value of ~3 μM.

Figure 5 summarizes the potency and relative efficacy of agonists that include conformationally restrictive rings. From these data, it is clear that placement of carboxylic acids on the same side of the average plane of the ring is preferred by the NR2 binding pocket. This is best illustrated in three sets of analogs with cyclopropyl, cyclobutyl, and cyclopentyl derivatives (Fig. 1 and 5). When carboxylic acids are placed on opposing sides of the ring, the molecules are either inactive or potency is lower than our threshold for analysis: L-CCG-I (8), *cis*-ACBD (10), *trans*-ACPD (16) (Fig. 1). By contrast, placement of both carboxylic acids on the same side of the ring creates agonists at all subunits, including L-CCG-IV

(46), *trans*-ACBD (47), and *cis*-ACPD (49) (Fig. 5). Similar results are found for CCG analogs of D-glutamate [(2*S*,1′*R*,2′*R*)-2-(carboxycyclopropyl)glycine (L-CCG-II), (2*S*,1′*S*,2′*R*)-2-(carboxycyclopropyl)glycine L-CCG-III; data not shown)].

It is noteworthy that of these conformationally restrictive rings, L-CCG-IV and *trans*-ACBD are 200- to 400- and 20- to 25-fold more potent, respectively, than *cis*-ACPD, suggesting that the conformational restrictions of the smaller cyclic analogs hold glutamate in near optimal positions for binding and receptor activation without inducing steric conflicts. Figure 6 shows these constrained glutamate analogs superimposed on the glutamate conformation extracted from the NR1/NR2A crystal structure. Note that L-CCG-IV places the γ-carboxyl in a position that is not attained by crystallographic glutamate ligand but is in fact closer to the polar residues at the top of helix F, whereas the cyclopropyl ring is not placed far from the carbons of the crystallographic agonist. We propose that this position further stabilizes binding of L-CCG-IV, enhancing its potency. By contrast, whereas the amino and carboxyl groups of *cis*-ACPD overlap well with the crystallographic glutamate position, *cis*-ACPD shows consider-

Agonist	Subunit	Efficacy (%)	EC50 (μM)	Hill slope	N	2A/2D EC50	Structure	EC50 (μM)
L-glutamate	2A	100	3.30	1.10	26		29	NR2D NR2C NR2B NR2A
	2B	100	2.86	1.32	9			
	2C	100	1.68	1.26	6			
	2D	100	0.51	1.55	11	7		
D-glutamate	2A	99	249	0.87	7		30	
	2B	123	156	1.01	10			
	2C	102	111	0.71	7			
	2D	110	42.3	1.26	7	6		
(2*S*,4*R*)-4-methylglutamate (SYM2081)	2A	72	144	1.19	12		31	
	2B	89	25.1	1.58	10			
	2C	71	18.2	1.27	10			
	2D	75	3.15	1.25	13	46		
(2*S*,4*S*)-4-methylglutamate	2A	78	404	0.88	7		32	
	2B	75	76.2	1.32	8			
	2C	80	87.4	1.23	10			
	2D	83	31.4	1.52	6	13		
DL-erythro-4-fluoroglutamate	2A	55	104	1.07	12		33	
	2B	76	76.7	1.22	11			
	2C	63	46.4	1.12	12			
	2D	84	22.0	1.67	10	5		
L-aspartate	2A	99	47.8	1.15	7		34	
	2B	78	14.3	1.34	7			
	2C	108	40.6	1.21	10			
	2D	91	11.6	1.77	8	4		
D-aspartate	2A	103	30	1.18	8		35	
	2B	91	10.1	1.18	7			
	2C	99	9.31	1.44	8			
	2D	90	2.10	2.11	7	14		
N-methyl-L-aspartate (NMLA)	2A	99	581	1.21	10		36	
	2B	69	127	1.41	9			
	2C	66	154	1.28	13			
	2D	75	40	1.60	8	15		
N-methyl-D-aspartate (NMDA)	2A	93	94.1	1.31	8		37	
	2B	78	29.5	1.16	7			
	2C	86	21.7	1.06	7			
	2D	92	7.30	1.53	7	13		

Fig. 3. The results of fitting concentration-response relationships for glutamate and aspartate analogs are displayed. Efficacy denotes the maximal current response to the test agonist relative to the maximal current response to glutamate, determined by least-squares fitting of the logistic equation to the data (see *Materials and Methods*). The ratio of the EC_{50} at NR2A compared with NR2D is given as an index of agonist selectivity between these subunits. The subunit-dependence of EC_{50} is displayed graphically for each agonist. DL-*erythro*-4-fluoroglutamate is a racemic mixture of all four stereoisomers.

Agonist	Subunit	Efficacy(%)	EC50 (μM)	Hill slope	N	2A/2D EC50	Structure	EC50 (μM)
L-homocysteinesulfinate	2A	91	73.2	1.25	12		38	NR2D NR2C NR2B NR2A
	2B	94	17.9	1.09	7			
	2C	70	13.7	1.62	10			
	2D	84	6.19	1.47	12	12		
D-homocysteinesulfinate	2A	89	36.2	1.25	8		39	
	2B	99	13.7	1.44	11			
	2C	92	7.88	1.24	10			
	2D	101	2.99	1.17	12	12		
L-homocysteate	2A	86	34.1	1.15	13		40	
	2B	90	8.09	1.14	13			
	2C	53	11.6	1.08	14			
	2D	69	3.35	1.62	10	10		
D-homocysteate	2A	92	180	1.21	10		41	
	2B	94	86.1	1.28	12			
	2C	74	108	1.00	10			
	2D	87	21.6	1.29	9	8		
L-cysteinesulfinate	2A	107	135	1.24	15		42	
	2B	81	103	1.32	10			
	2C	103	21.7	1.36	11			
	2D	98	9.20	1.18	11	15		
L-cysteate	2A	95	557	1.14	8		43	
	2B	77	182	1.49	7			
	2C	82	79.5	1.45	10			
	2D	83	29.5	1.78	7	19		
D-cysteate	2A	31	216	1.51	20		44	
	2B	67	214	1.40	25			
	2C	114	581	0.94	18			
	2D	97	101	1.01	14	2		

Fig. 4. The results of fitting concentration-response relationships for sulfur containing glutamate and aspartate analogs are displayed. Efficacy denotes the maximal current response to the test agonist relative to the maximal current response to glutamate, determined by least-squares fitting of the logistic equation to the data. The ratio of the EC_{50} at NR2A compared with NR2D is given as an index of agonist selectivity between subunits. The subunit-dependence of EC_{50} is displayed graphically for each agonist.

ably less potency than glutamate, which may reflect steric clash between the large cyclopentyl ring and residues within the agonist binding pocket. *trans*-ACBD is intermediate in potency potential with good overlap to crystallographic agonist features, which may indicate an intermediate potential for steric interference relative to L-CCG-IV and *cis*-ACPD.

Structural Determinants of Agonist Binding. Only NR2A and NR2D show a significant difference in potency among all agonists examined ($p < 0.004$; Kruskal-Wallis one-factor rank ANOVA; Tukey test). For example, L-glutamate showed a 6.5-fold decrease in EC_{50} (i.e., increase in potency) at NR1/NR2D compared with NR1/NR2A. Furthermore, a 4-substituted L-glutamate analog, SYM2081 (31), showed 46-fold higher potency at NR1/NR2D than at NR1/NR2A (Fig. 3). It is noteworthy that the 4-stereoisomer complementary to SYM2081 that places the 4-methyl group in a different configuration [2*S*,4*S*-4-methylglutamate (32)] shows only modest difference in potency between receptors containing the NR2A and NR2D subunits (Fig. 3). Similar to L-glutamate, the EC_{50} value of (2*S*,4*S*)-4-methylglutamate is 13-fold lower for NR2D versus NR2A. These data suggest that the agonist-binding pocket for NR2D is more tolerant of the 4-methyl substitution in the R configuration than NR2A.

To identify the structural features that are responsible for the difference in glutamate and SYM2081 potency between NR2A and NR2D subunits, we generated chimeric NR2 subunits by replacing the two regions of the cDNA that give rise to the agonist binding domain (S1 and S2) of NR2A with the corresponding portion of NR2D (Fig. 7A). The S1 domain gives rise to most of Domain1, whereas the S2 region of the polypeptide chain encodes most of Domain2 (discussed below). Replacement of either S1 or S2 resulted in a substantial shift in glutamate potency between NR2A and NR2D (Table 1 and Fig. 7B). Replacement of NR2A-S1 alone with NR2D-S1 caused a somewhat larger shift in potency for SYM2081 than for replacement of NR2D-S2 (Fig. 7C). Replacement of both S1 and S2 transfers the full difference in SYM2081 potency between NR2A and NR2D. Similar results were obtained using *cis*-ADA (48), L-homocysteate (40), and D-homocysteate (41) to activate wild-type and chimeric receptors (n = 5–13, data not shown). These data suggest that although differences in agonist potency are controlled entirely by the S1–S2 ligand binding domain, multiple structural determinants seem to control the differential agonist potency at NR2A and NR2D, and these determinants are distributed between S1 and S2 segments of the agonist binding domain. That is, structural elements in both S1 and S2

Agonist	Subunit	Efficacy (%)	EC50 (μM)	Hill slope	N	2A/2D EC50	Structure	EC50 (μM)
(*RS*)-(tetrazol-5-yl)glycine	2A	98	1.72	1.13	7		45	
	2B	97	0.518	1.39	6			
	2C	89	0.491	1.27	6			
	2D	78	0.0993	1.89	7	17		
(2*S*,3*R*,4*S*)-2-(carboxycyclopropyl) glycine (L-CCG-IV)	2A	99	0.262	1.12	9		46	
	2B	123	0.0834	1.05	12			
	2C	90	0.110	1.10	12			
	2D	111	0.0360	1.30	12	7		
trans-1-aminocyclobutane-1,3-dicarboxylate (*trans*-ACBD)	2A	91	3.06	1.14	7		47	
	2B	81	0.995	1.25	12			
	2C	67	1.15	1.26	11			
	2D	81	0.512	1.36	9	6		
cis-azetidine-2,4-dicarboxylic acid (*cis*-ADA)	2A	100(fix)	892	1.23	6		48	
	2B	95	217	1.41	6			
	2C	81	80.0	1.23	6			
	2D	136	32.0	1.33	13	~28		
(1*R*,3*R*)-aminocyclopentane-*cis*-1,3-dicarboxylate (*cis*-ACPD)	2A	76	60.9	1. 40	8		49	
	2B	75	21.2	1.66	8			
	2C	49	22.4	0.97	9			
	2D	77	10.5	1.27	6	6		
homoquinolinate	2A	75	22.1	1.32	23		50	
	2B	96	16.1	1.36	13			
	2C	51	81.1	1.19	15			
	2D	88	32.3	1.55	16	1		
ibotenate	2A	99	161	0.90	11		51	
	2B	89	26.4	1.05	20			
	2C	72	40.0	1.15	10			
	2D	78	13.0	1.95	14	12		
(*R*)-NHP4G	2A	33	145	1.24	8		52	
	2B	76	61.0	1.48	8			
	2C	54	117	1.15	8			
	2D	77	48.0	1.41	9	3		

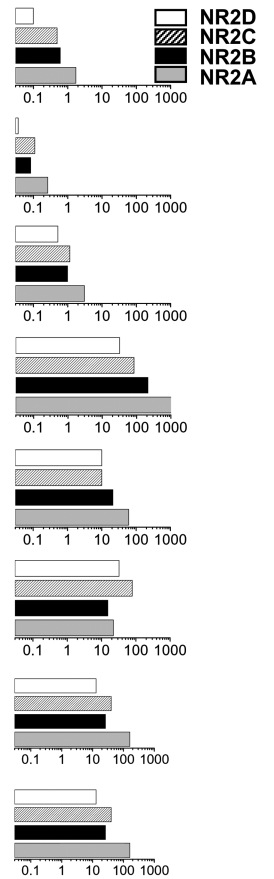

Fig. 5. The results of fitting concentration-response relationships for conformationally constrained glutamate and aspartate analogs are displayed. Efficacy denotes the maximal current response to the test agonist relative to the maximal current response to glutamate, determined by least-squares fitting of the logistic equation to the data. The ratio of the EC_{50} at NR2A compared with NR2D is given as an index of agonist selectivity between subunits. The subunit-dependence of EC_{50} is displayed graphically for each agonist. For *cis*-ADA, the low potency prevented determination of the maximal response at NR2A. We measured the concentration response relationship for 10 μM to 3 mM *cis*-ADA (87% response of maximal glutamate). We then fixed the maximum response to *cis*-ADA as 100% that of glutamate, and fitted the curve to estimate the potency, which was 892 μM. If *cis*-ADA had a higher relative efficacy than glutamate, its potency would be lower than what is reported here.

regions underlie the NR2D subunit preference of glutamate and SYM2081. These data also suggest that if differences in gating between NR2A and NR2D influence the measured EC_{50} values, these gating differences must either be contained in or controlled by the S1–S2 ligand-binding domain.

Molecular Dynamics Simulation of Glutamate-Bound NR1/NR2A and NR1/NR2D. NR2A and NR2D share strong sequence identity yet show different agonist selectivity. To better understand the structural basis of differential agonist potency between NR2A and NR2D subunits, we exploited recent crystallographic data on the NR1/NR2A dimer to build a hydrated model of the NR1/NR2A dimer and a hydrated homology model of the NR1/NR2D dimer (Fig. 8A). These two models were subject to MD simulations (see *Materials and Methods*). Glutamate remained stably docked into binding sites for both NR2A and NR2D throughout the full 10-ns simulation, maintaining a set of contacts with many similar residues that have been described previously for amino acid binding in NR1 and NR2A NMDA receptor subunits (Anson et al., 1998; Furukawa and Gouaux, 2003; Chen et al., 2005; Furukawa et al., 2005) as well as other glutamate receptor subunits (Mayer and Armstrong, 2004). Comparison of the root-mean-square deviation (RMSD) of backbone atoms throughout each of the 10-ns simulations demonstrates that each simulation had stabilized around an equilibrium structure by 2 ns at 300 K. Good agreement in backbone alignment is found when comparing the 2A5T crystal structure to an average of the final 2 ns of the NR1/NR2A-glutamate simulation (Fig. 8, B and C) for most of the dimer. Overall, the root-mean-square (RMS) deviations of a Cα alignment of the crystal structure to the average structure of NR2A and NR2D were 2.74 and 2.87 Å, respectively. Comparison of crystallographic water molecules near the ligand to the water environment around the ligand in the NR1/NR2A simulations revealed positionally equivalent water

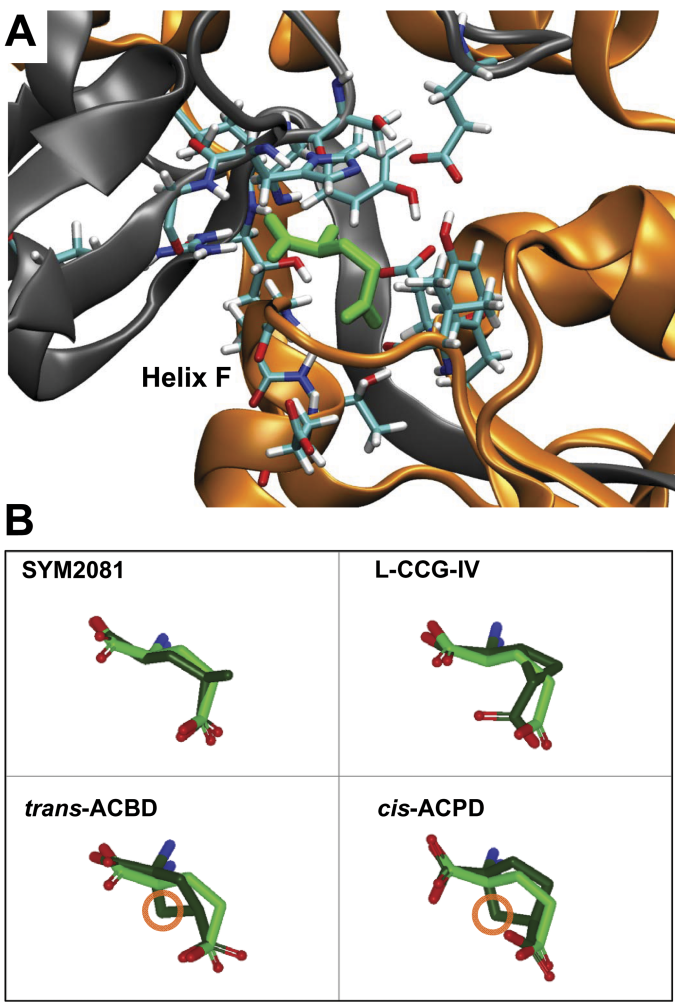

Fig. 6. A, the crystallographic binding site of NR2A (2A5S) with glutamate ligand shown in green and neighboring residues displayed to demonstrate steric constraints of the binding site. B, superposition of the crystallographic conformation of glutamate bound to NR2A (light green) and the best aligned structure of SYM2081 and several constrained analogs (see *Materials and Methods*). Note how the two larger cyclic analogs (*trans*-ACBD and *cis*-ACPD) present a potential for steric clash (orange circle) with the top of helix F when superimposed onto glutamate.

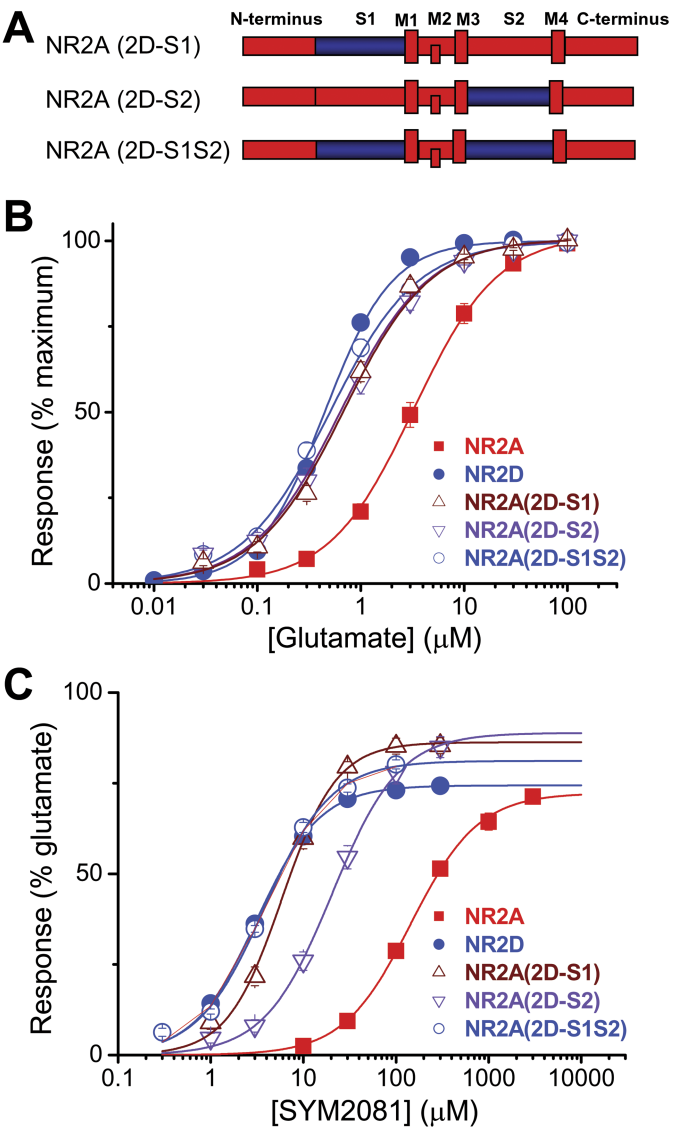

Fig. 7. A, a linear map for each of the NR2A/NR2D chimeras is shown coded for NR2A (red) and NR2D (dark blue). B, composite concentration-response curves are shown for glutamate at wild-type NR1/NR2A, wild-type NR1/NR2D, and each of the three chimeric receptors. Each curve was constructed from 26 to 30 oocytes. C, composite concentration-response curves are shown for SYM2081 at wild-type NR1/NR2A, wild-type NR1/NR2D, and each of the three chimeric receptors. Each curve was constructed from 8 to 13 oocytes. Error bars (S.E.M.) are shown when larger than symbol size.

molecules that were present throughout the simulation despite fluctuations and movement of some binding-site residues from their crystallographic positions. That is, the molecular dynamics simulation predicted stabilized water in the binding pocket, as is found in the crystal structure. This suggests the simulations correctly represent atomic interactions in the NR1/NR2A binding pocket.

Comparison of the average NR1/NR2A and NR1/NR2D structures from the final 2 ns of the MD simulations further reveals structural differences. Figure 8, D and E, shows that the NR1 domains in the averaged structures from the simulations of the two complexes align better than the NR2 domains (1.98 Å RMSD for NR1 versus 2.75 Å RMSD for NR2 based on Cα alignment), as expected because of sequence variation in NR2. The upper domain of the agonist binding core (referred to as Domain1, Fig. 8A) is composed largely of sequence from S1 region of the polypeptide chain, with a portion of S2 region of the polypeptide chain (Fig. 8A). Likewise, the lower domain (referred to as Domain2) is largely composed of residues from the S2 portion of the polypeptide chain with a portion of S1. Average structures of NR2A and NR2D show the greatest differences in the surface loops as well as the Domain2 (Fig. 8, D and E). Hingefind analysis (see *Materials and Methods*) reveals a modest counterclockwise rotation (~15°) of the outer portion of the Domain2 in NR2D (Fig. 8D) compared with the same region in NR2A.

TABLE 1
Glutamate and SYM2081 potency at NR2A/D chimeric receptor constructs

Receptor Construct	Glutamate				SYM2081			
	EC_{50}	EC_{50} NR2(Chim)/ NR2D(WT)	Hill Slope	*n*	EC_{50}	EC_{50} NR2(Chim)/ NR2D(WT)	Hill Slope	*n*
	μM				*μM*			
Wild-type NR2A	3.3	7	1.1	26	144	46	1.2	12
Wild-type NR2D	0.49		1.5	30	3.2		1.3	13
NR2A(2D-S1)	0.68	1.4	1.0	27	5.9	1.9	1.6	8
NR2A(2D-S2)	0.64	1.3	1.0	26	20	6.4	1.3	8
NR2A(2D-S1S2)	0.50	1.0	1.0	26	3.8	1.2	1.2	6

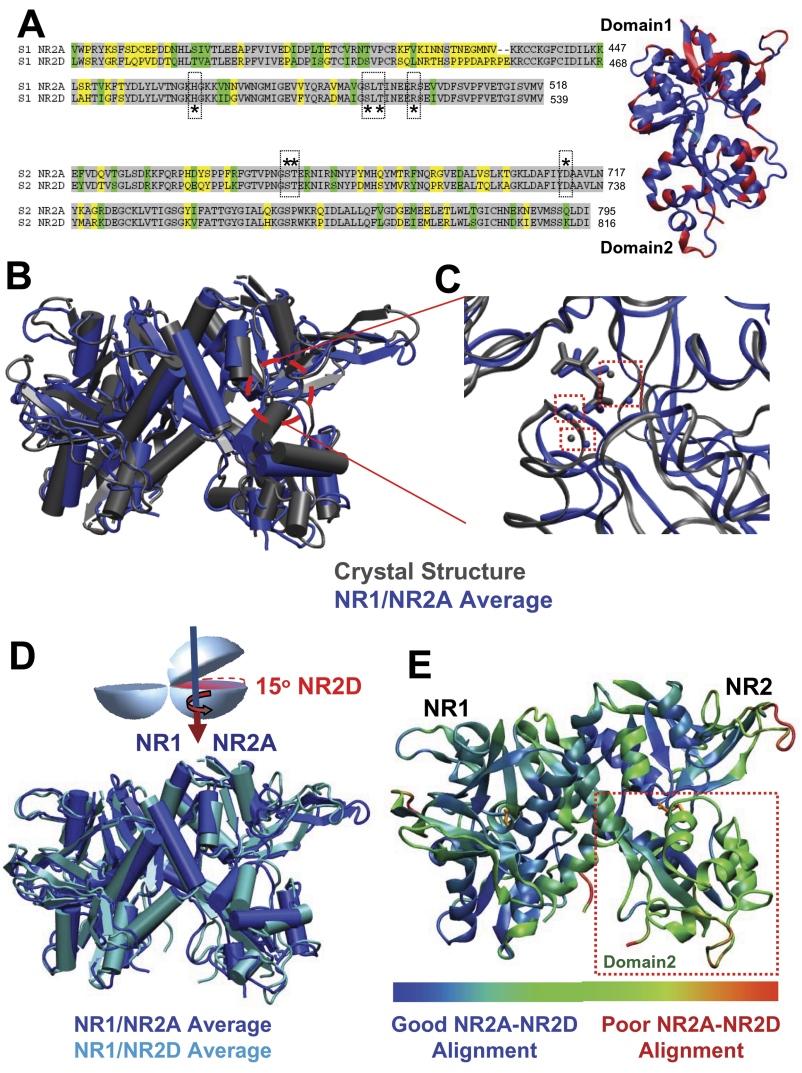

Fig. 8. A, sequence alignment between NR2A and NR2D S1/S2 domains is shown with conserved residues in gray, conservative substitutions in green, and divergent residues in yellow. Right, the NR2A backbone structure colored to show conserved residues (blue) and divergent regions (red). Note that the atomic contact residues (denoted by *) within the ligand binding pocket are conserved. B, the backbone alignment between crystal structure of NR1/NR2A (2A5S, Furukawa et al., 2005, gray) and representative structure from the latter stage simulation of hydrated NR1/NR2A (blue) is shown. C, an enlarged view of the NR2A glutamate binding pocket shows the similar positioning (broken red boxes) of the crystallographic (gray) and long lived waters in simulation (blue). D, superposition of averaged structures after 10 ns of molecular dynamics simulations for hydrated crystallographic NR1/NR2A (blue) and hydrated homology model of NR1/NR2D (cyan). The outer portion of NR2D domain2 appears to rotate counter-clockwise (from top) with respect to NR2A. E, backbone of NR1/NR2A color-coded to reflect superposition of alpha carbons for average structures after molecular dynamics of NR1/NR2A and NR1/NR2D (blue, good superposition; red, poor superposition; green, intermediate superposition). Apart from loops, Domain2 of NR2 is the most divergent region in terms of superposition.

Differential Atomic Contacts within the NR2 Binding Pockets. Whereas the residues comprising the agonist binding pockets of NR2A and NR2D are identical (Fig. 8A), subtle differences in positioning of both ligand and binding pocket residues developed over the course of the simulations. Most contacts were preserved between the subtypes, yet our simulations suggest that at 300 K (i.e., approximately room temperature), each interacting region of the ligand (α-carboxyl, amino, and γ-carboxyl) developed at least one differing interaction between the models of NR2A and NR2D. Some of these contacts in NR2A model differ from those described in the crystal structure, which could reflect temperature, thermal motion, or assumptions inherent in the simulations (see *Discussion*). In the NR1/NR2A simulation, the γ-carboxyl of glutamate forms consistent hydrogen bonds with the backbone of Ser670, the backbone and side chain of Thr671 (e.g., Chen et al., 2005), and the backbone of Asp712 (Fig. 9A). In simulations of NR1/NR2D, the analogous NR2D residues Ser691 and Thr692 also make direct contacts with the γ-carboxyl of glutamate (not shown). However, there is an additional contact with the side chain of Tyr732 (Fig. 9B). The amino group of glutamate shares hydrogen bonding with the side chains of Ser492, Asp712, and Tyr742 (Ser513, Asp733, and Tyr763 in NR2D) between the subtypes (Fig. 9, A and B). In addition, the amino group of glutamate also interacts with the backbone of NR2D Ser513 (Fig. 9B). Simulations of both NR1/NR2A and NR1/NR2D showed strong interactions between the α-carboxyl and the side chain of Arg499 (Arg520 NR2D), the side chain and backbone of Thr494 (Thr515 NR2D) and the side chain of Ser670 (Ser691 NR2D; data not shown). In NR2A, a consistent hydrogen bond is also observed between the backbone amide of Ser670 and the α-carboxyl group of glutamate. However, in NR2D, this amide interacts exclusively with the γ-carboxyl of glutamate (data not shown). We speculate, based on the molecular dynamics simulation, that the different atomic contacts influence the position of glutamate within the binding pocket, which differs between NR2A and NR2D (Fig. 9C).

Differential Interdomain Atomic Contacts within the NR2 Binding Domains. Predicted changes in the agonist binding pocket discussed above occur concurrently throughout the simulations with alteration of some of the interdomain contacts between Domain1 and Domain2 (Fig. 10). Both NR2A and NR2D simulations show persistent hydrogen bonding between the side chains of Glu498 to Arg673 in NR2A (Glu519–Lys694 in NR2D) and Thr512 to Asp712 in NR2A (Thr533–Asp733 in NR2D; Fig. 10). However, several other interdomain contacts varied between the two NR2 subunits. For example, in the NR2A simulation, the hydrogen bonding between Glu394 and Tyr711 was stable throughout the entire simulation (Fig. 10A, bottom), but in NR2D the equivalent interaction (Glu413 to Tyr732) was lost around 5 ns and was never reformed, with Tyr732 forming direct interactions with glutamate as described above. Thus, glutamate participates in interdomain bridging interactions of Tyr732 in NR2D. In addition, simulations revealed that NR2D had a persistent interaction between Arg414 and Tyr739 (Fig. 10B, bottom) that does not occur in simulations or crystal structure of NR2A because the residue in the analogous position as the NR2D arginine is NR2A Ala395. Finally, Lys486 formed consistent interaction with both the side chain and backbone oxygens of Asn689 in the NR2D simulation (Fig. 10B, bottom). The analogous Lys465 in NR2A forms a few intermittent contacts with equivalent residues, but no stable interaction was formed over the course of the simulation. These simulations suggest that the glutamate-bound NR2D subunit maintains a number of stable contacts seen in NR2A, and shows additional unique interdomain contacts that do not appear in NR2A. These new interdomain hydrogen bonds, each potentially contributing stabilization of 3 to 5 kcal/mol, should provide more than enough energy to increase glutamate potency by 10-fold.

Mutagenesis of NR2A and NR2D Agonist Binding Domains. To probe the validity of our simulations that identified several different agonist-protein contacts for NR2A versus NR2D, we used site-directed mutagenesis to change a series of residues in analogous positions in NR2A and NR2D. Table 2 summarizes the changes in glutamate EC_{50} values for all of these mutations. Consistent with our simulations and the high degree of sequence similarity, these data suggest that most of the atomic determinants of agonist binding between NR2A and NR2D are similar. Note that the ratio of

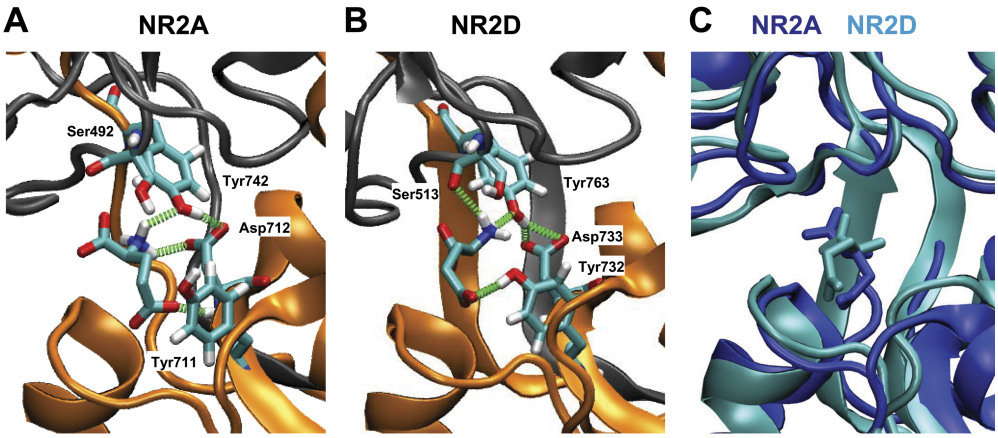

Fig. 9. Agonist binding site interactions are shown in these representative images from the simulations of glutamate agonist bound to NR1/NR2A (A) and NR1/NR2D (B). Only residues divergent from known crystallographic atomic contacts (Chen et al., 2005; Furukawa et al., 2005) are shown. Differences among atomic contacts between simulations include a change of the Tyr711 from its apparent role as an interdomain hydrogen-bonded bridge to Glu394 in NR2A (Furukawa et al., 2005) to a hydrogen bonding partner with the γ-carboxyl of the glutamate agonist for the corresponding residue Tyr732 in NR2D. In addition, Ser513 backbone seems to participate in hydrogen bonding of the amino group of the agonist in NR2D but not in NR2A. C, superposition of NR2A (blue) and NR2D (cyan) binding pockets shows the different position of the glutamate backbone in the binding pocket.

EC_{50} values for mutant and wild type receptors is similar for each pair of NR2A/NR2D mutations, with the exception of NR2ATyr711/NR2DTyr732. As expected from the rearrangement of NR2D Tyr732 predicted by our simulations, the largest divergence in effect of mutations within the binding pocket was observed for equivalent mutations NR2A Y711F and NR2D Y732F (Table 1). We observed a 100-fold difference in the relative change in EC_{50} values, with a 45-fold increase in EC_{50} observed for NR2A(Y711F) compared with a 2.5-fold decrease in EC_{50} measured for NR2D(Y732F). This tyrosine residue showed markedly different behavior in the simulations, with Tyr711 in NR2A forming a cross-domain interaction, whereas the analogous Tyr732 in NR2D switched to hydrogen bonding to the γ-carboxyl of glutamate. We speculate that NR2A(Y711F) mutation leads to unfavorable steric interactions in the binding pocket because the interdomain contact is lost, and the phenylalanine is free to swing into binding pocket. The different position of agonist and the Tyr732 residue in the NR2D pocket might mitigate this potential steric clash in NR2D(Y732F).

Mutagenesis results also support the idea that the differential interdomain contacts identified in NR2D but lacking in NR2A contribute to the EC_{50} value. Maier et al. (2007) have already shown that mutations affecting interdomain interactions can have a strong effect on binding. We evaluated in NR1/NR2A each of two interdomain contacts shared by NR2D and NR2A (Glu498:Arg673, Thr512:Asp712). Mutation of the Domain2 contributor NR2A(D712A) produced a

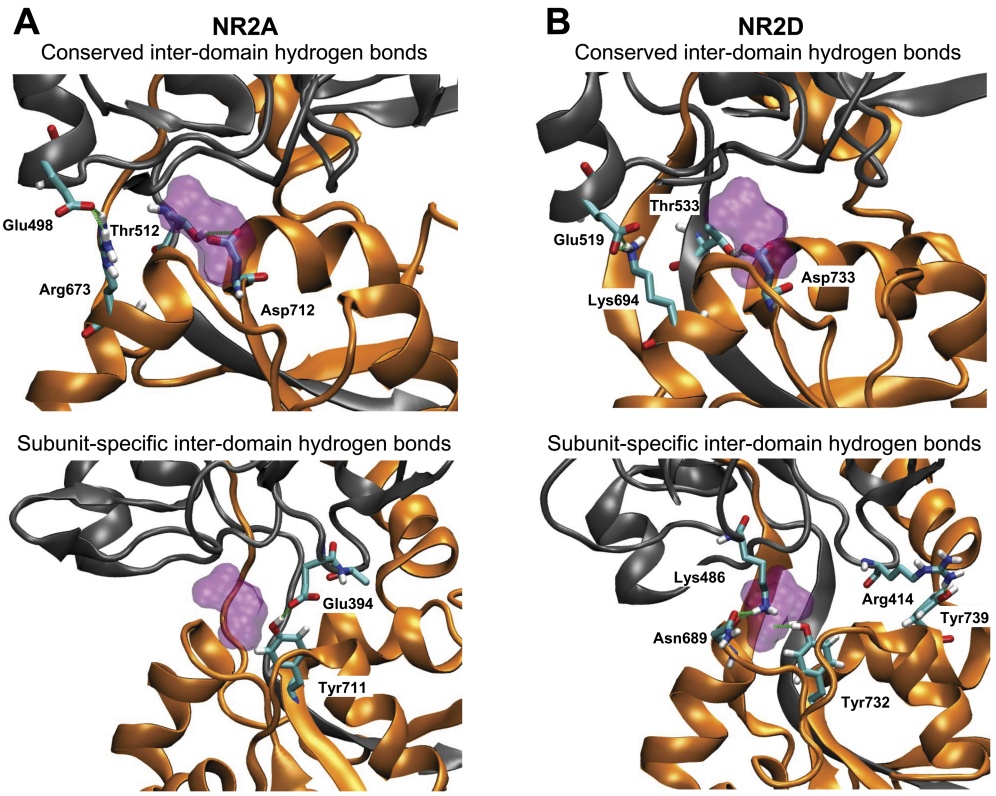

Fig. 10. Differential interdomain hydrogen bonds are shown between Domain1 (gray) and Domain2 (bronze) in the NR2A (A) and NR2D (B). Top, cross-domain hydrogen bonding that is conserved between the two subunits. Bottom, cross-domain hydrogen bonds that are not conserved between the two subunits. The surface of the bound glutamate ligand is shown in purple for reference.

TABLE 2
Effect of binding site mutations on glutamate potency
NR indicates mutant receptor showed no response when tested at glutamate concentrations up to 30 mM. N.D. indicates that the ratio of EC_{50} for mutant to EC_{50} for wild-type could not be determined. Shift 2A/Shift 2D is the ratio of the EC_{50} Mut/WT for NR2A and EC_{50} Mut/WT for NR2D.

NR2A Mutation	EC_{50}	EC_{50} Mut/WT	Hill Slope	*n*	NR2D Mutation	EC_{50}	EC_{50} Mut/WT	Hill Slope	*n*	Shift 2A/Shift 2D
	μM					*μM*				
Wild-Type NR2A	3.3		1.1	26	Wild-Type NR2D	0.49		1.5	30	0.7
H466A[a]	490	140	1.5		H487A	76	150	1.2	8	0.9
H466F[a]	46.2	14	1.7		H487F	2.3	4.7	2.0	7	3.0
G467V	>3000	N.D.		6	G488V	>3000	N.D.		6	
R499A	>3000	N.D.		12	R520A	>3000	N.D.		6	
R499K	>3000	N.D.		12	R520K	>3000	N.D.		12	
S670A	1.6	0.5	1.2	11	S691A	0.2	0.4	1.2	8	1.3
S670G[a]	421	120	1.4		S691G	46	94	1.2	6	1.3
T671A[b]	2967	900	1.3		T692A[c]	703	1400	1.5		0.6
Y711F	143	45	1.3	6	Y732F	0.20	0.4	1.7	12	113
D712A	>3000	N.D.		6	D733A	NR	N.D.		8	
Y742F	40	12	1.3	8	Y763F	6.1	12	2.2	6	1.0

Data from previous studies are included for comparison:
[a] Chen et al. (2005).
[b] Anson et al. (1998).
[c] Chen et al. (2004).

dramatic reduction in potency; EC_{50} could not be determined, and was higher than 3 mM (n = 6) (Table 2). By contrast, mutation of the Domain2 contributor to the other interdomain contact, NR2A(R673A), produced little effect, paradoxically enhancing potency 5-fold (EC_{50}, 0.6 μM, n = 8). Table 2 shows the importance of the other interdomain contact in NR2A (Glu394:Tyr711), with the NR2A(Y711F) mutation shifting EC_{50} by 45-fold. These data are consistent with the idea that the interdomain hydrogen bonds can stabilize the closed conformation and thus influence the energetics underlying agonist binding to the NR2A subunit. However, Tyr711 and Asp712 are both part of the glutamate binding pocket, so their effect cannot be fully differentiated from an effect on ligand binding.

We subsequently evaluated four pairs of identified interdomain contacts in NR2D (Lys486:Asn689, Arg414:Tyr739, Glu519:Lys694, Thr533:Asp733). In each case, mutation of at least one the pairs of residues increased EC_{50} (decreased potency) (Table 3). The mutant subunits NR2D(E519A), NR2D(R414A), and NR2D(N689A) all decreased glutamate potency at NR1/NR2D receptors by ~4-fold or more. Two mutations, NR2D(K694A) and NR2D(K486A), had no negative effect on potency. One mutation, NR2D(Y739A), unexpectedly increased potency, although the conservative substitution NR2D(Y739F) had no effect. Replacement of the tyrosine with an alanine may be favorable because it removes steric clash in a hydrophobic region between the two domains. Together, these data all support the idea that the interdomain contacts contribute to enhanced potency of the NR2D subunit.

Because experimentally determined EC_{50} values are influenced both by rate constants governing agonist binding and channel gating, mutations that alter gating also influence measured EC_{50} values (Colquhoun, 1998). To assess the potential effects of the NR2A mutations studied in Table 2 on gating, we estimated the open probability by evaluating the reciprocal of the potentiation observed by MTSEA covalent modification of NR1(A652C)/NR2A (Fig. 11A) (Jones et al., 2002; Chen et al., 2005; Yuan et al., 2005). We tested the effect of MTSEA on residues in NR2A that we probed with mutagenesis for which a clear maximally effective concentration of glutamate could be determined. Figure 11B shows that there was no significant alteration in the degree of potentiation by 0.2 mM MTSEA (2.1- to 2.7-fold potentiation of NR2A mutants compared with 2.3-fold of WT NR2A; ANOVA), which we interpret to reflect a similar open probability for mutant and wild-type receptors. These data are consistent with a previous report for NR2A(S670G) and NR2A(T671A) (Anson et al., 2000; Chen et al., 2005; Wyllie et al., 2006), as well as findings that NR2A(H466A) has little effect on gating (Maier et al., 2007). In addition, these data suggest that the changes observed in potency shown for NR2A mutations in Table 2 probably reflected changes within the binding pocket rather than gating changes. We are unable to quantify open probability for NR2D using this method because the small response of NR1(A652C)/NR2D and the large potentiation when channels are locked open by coapplication of MTSEA and glutamate makes determination of the degree of potentiation variable (Yuan et al., 2005).

Analysis of SYM2081-Bound NR1/NR2. The glutamate analog SYM2081 (31) has a 4-methyl substituent adjacent to the γ-carboxyl group of glutamate and activates NR2A-D receptors with efficacy ranging between 0.71 and 0.89 that of glutamate. Both efficacy and microscopic association and dissociation constants governing agonist binding influence measured EC_{50} values. Given the similar efficacy of SYM2081 and glutamate, the 46-fold difference in potency between NR2A and NR2D suggests differences in the binding

TABLE 3
Interdomain mutations shift glutamate potency for NR2D

NR2D Mutation	H-Bond Partner	EC_{50}	EC_{50} Mutant/ Wild-Type	Hill Slope	n
		μM			
Wild-type NR2D		0.49		1.5	30
R414A	Y739	1.9	3.8	1.8	6
R414K	Y739	0.82	1.7	1.7	6
K486A	N689	0.48	1.0	1.4	6
E519A	K694	2.5	5.0	1.6	6
N689A	K486	3.1	6.4	1.6	6
K694A	E519	0.29	0.6	1.5	8
K694R	E519	0.36	0.7	1.6	6
D733A	T533	N.R.			8
Y739A	R414	0.06	0.1	1.1	5
Y739F	R414	0.6	1.3	1.5	6

N.R., mutant showed no response when tested at glutamate concentrations up to 30 mM.

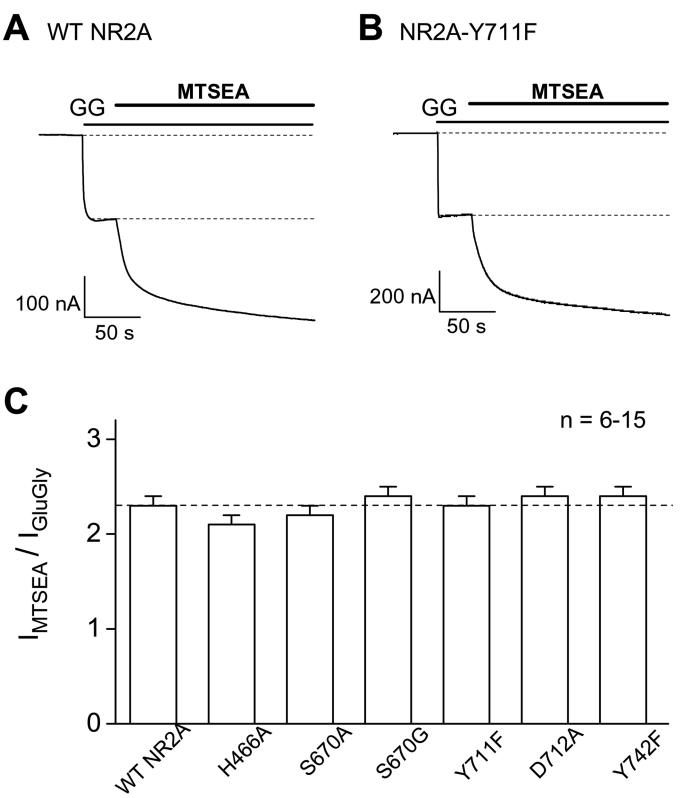

Fig. 11. A, current recording from NR1(A652C)/NR2A in response to application of a maximally effective concentration of glutamate before and during application of the cysteine-labeling reagent MTSEA. We interpret the potentiation of current as an indication of the consequence of shifting open probability to near 1.0. Thus, the degree of potentiation is inversely related to the open probability at rest for the receptor. B, current recording from NR1(A652C)/NR2A(Y711F) before and during application of MTSEA. C, summary of potentiation determined from a representative mutation at each residue tested in Table 2 for which we could determine a maximally effective concentration of glutamate. For all, there was no significant difference from wild type NR2A ($p > 0.05$; 1 factor ANOVA, Tukey test). Recordings were made from between 6 and 17 oocytes per mutation.

pocket rather than effects on gating. Inspection of the glutamate conformations extracted from the averaged structures of NR1/NR2A and NR1/NR2D simulations suggests that the agonist occupies different space in NR2A compared with NR2D (Fig. 9C). We therefore sought to explore whether the potency differences of SYM2081 could be understood in terms of structural predictions from our simulations. Toward this end, we performed molecular dynamics simulations on SYM2081 placed into the binding pocket in the position of glutamate (Fig. 12, A and B). The results showed that the methyl group of SYM2081 clashes with Tyr711 in NR2A, which results in a push or rotation of the agonist in the pocket during the simulation. The change in agonist position leads to a loss of contact between SYM2081 and Arg499, after which the methylated glutamate became progressively less stably bound in NR2A. By contrast, SYM2081 docking in the NR2D pocket is very stable throughout the simulation, persisting with all of the same atomic contacts acquired by glutamate in the binding pocket (e.g., Fig. 9B). This stability reflects differences in the binding pocket and ligand positioning in NR2D, which directs the 4-methyl group toward a part of the pocket without steric crowding. These simulations support the experimental results showing SYM2081 to be more potent at NR2D than NR2A. To further test this possibility, we evaluated the effects of the mutations NR2A(Y711F) and NR2D(Y732F). It is noteworthy that these mutations now have the opposite effect on the potency of SYM2081 by comparison with glutamate. NR2A(Y711F) shows a smaller shift in potency on NR2A (EC_{50} increased 7-fold, $n = 11$) compared with NR2D(Y732F), which causes a large shift in potency on NR2D (EC_{50} increased 29-fold; $n = 10$). These data are again consistent with the predicted differential atomic contacts of this residue in NR2A and NR2D. They also are consistent with a different interaction of SYM2081 in each pocket relative to L-glutamate.

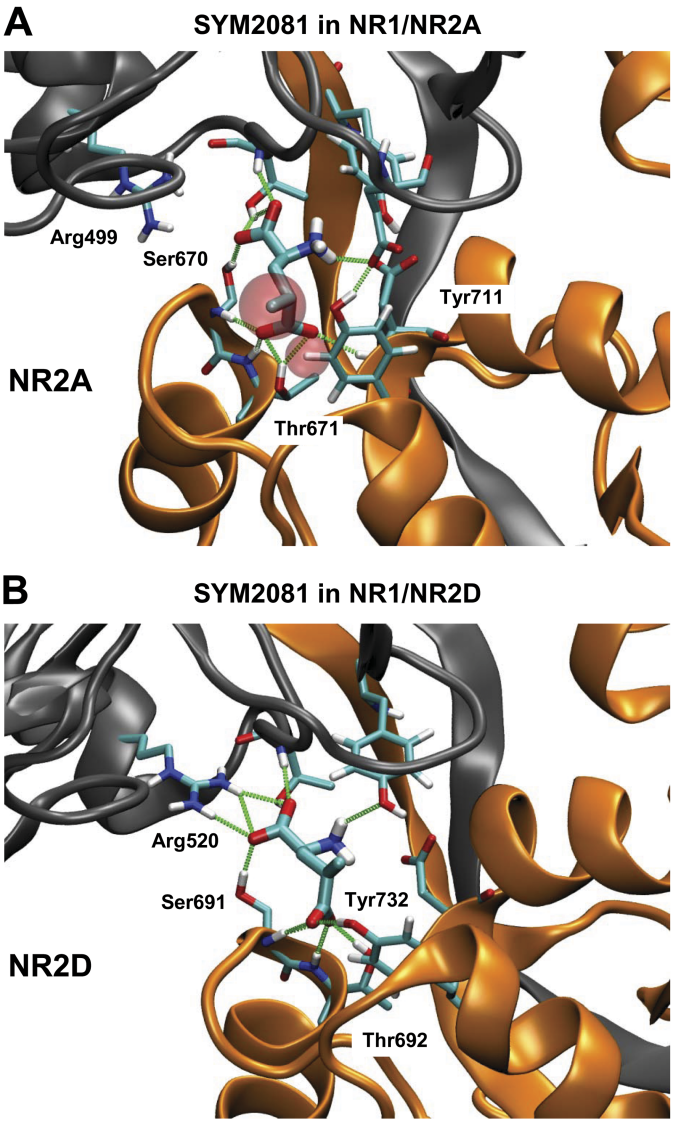

Fig. 12. Top, frame from early in the molecular dynamics simulation of SYM2081 in NR1/NR2A (around 1.7 ns). Note the steric contact (illustrated by transparent red spheres) between the methyl group of SYM2081 and Tyr711. This repeated collision seems to prevent the α-carboxyl of SYM2081 from contacting Arg499. Bottom, stably bound SYM2081 in the NR1/NR2D binding pocket after approximately 5 ns of MD simulation. The difference in binding pose for SYM2081 as well as the transition of Tyr732 to an interaction with the γ-carboxyl of SYM2081 results in little steric conflict for the 4-methyl group and a stable contact between the α-carboxyl and Arg520.

Discussion

In this study, we report the subunit-specific agonist potency and relative efficacy for a wide range of compounds at all four NR1/NR2 heterodimeric NMDA receptors. Four notable features emerge from the comprehensive comparison of NMDA receptor agonists. First, compounds with ring systems that place conformational constraints on agonist flexibility show strong stereoselectivity. For example, L-CCG-IV (46) was the agonist with the highest potency in the data set, but the stereoisomer L-CCG-I (*8*) (differing at one stereogenic site) is inactive. Second, the general rank order of potency for agonists across the NR2 subunits is NR2D > NR2C ~ NR2B > NR2A, with a notable exception being homoquinolinate, which was more potent at NR2A and NR2B (Buller and Monaghan, 1997). This order of potency correlates well with the deactivation time of current responses after a brief synaptic-like pulse of glutamate (Monyer et al., 1994; Vicini et al., 1998), presumably because the relatively slow unbinding rate of agonist from receptors contributes to (but does not solely control) the deactivation time course. The ratio of potency for each agonist at NR2D relative to NR2A provides an index of subunit selectivity.

Third, 4-methyl substituted glutamate, (2*S*,4*R*)-4-methylglutamate or SYM2081 (31), shows a 46-fold higher potency for NR2D over NR2A, suggesting that different steric constraints between NR2A and NR2D may exist within the binding pocket. Use of SYM2081 to evaluate structural determinants of selectivity suggests that both domains of the bilobed agonist binding site appear to control SYM2081 and glutamate potency at NR2A and NR2D. Molecular dynamics simulations suggest that the 4-methyl substituent clashes in NR2A with Tyr711, leading to a rotation of the glutamate backbone that compromises interactions with Arg499. By contrast, the 4-methyl substituent fits into a crevice in NR2D, allowing stable docking. One enantiomer of SYM2081, (2*S*,4*S*)-4-methylglutamate (32), that places the 4-methyl substituent on the other side of glutamate relieves steric clash with Tyr711 in NR2A during MD simulation. This compound showed less difference in potency between

NR2A and NR2D (13- versus 46-fold), supporting our interpretation. One additionally important implication of the data are that the EC_{50} for SYM2081 at NR2D (3 μM) is in the same concentration range as that shown to interact with some kainate receptors (Bleakman, 1999). Thus, the ability of SYM2081 to activate NR2D-containing NMDA receptors raises a caveat to the use of SYM2081 as a selective kainate receptor probe in neurons that might also express NR2D subunits.

Fourth, there is no correlation across all agonists tested between EC_{50} and efficacy, suggesting that some of the molecular determinants of agonist binding differ from the determinants coupling agonist binding to gating. This is not surprising because efficacy is likely to be strongly (but not exclusively) controlled by gating elements that lie closer to the ion conducting pore, whereas potency will be strongly (but not exclusively) influenced by structural elements such as atomic and interdomain contacts within the binding pocket. However, recent findings suggest that certain regions of the agonist binding domain can influence gating (Hansen et al., 2005; Maier et al., 2007). Chimeric NR2A with the S1-S2 regions of NR2D inserted has almost identical agonist potency to the NR2D wild-type, supporting the idea that the agonist potency is determined predominantly by the ligand binding domain independent of the ion channel-forming portion of the receptor or the amino- or carboxyl-terminal domains. Results with chimeric receptors show that residues on both sides of the bilobed agonist binding domain contribute to agonist preferences, a finding that is consistent with known agonist contact residues. It is noteworthy that most agonists have lowest efficacy relative to glutamate at NR2C, suggesting that further studies with NR2C may provide insight into the structural basis for partial agonism at NMDA receptors.

Structural Determinants of Agonist Potency at NR2 Subunits. We have used molecular dynamics simulations to gain insight into the molecular basis of subunit preferences for NR2D over NR2A subunits. In this endeavor, we employed the dimeric NR1/NR2A crystal structure, and built a hydrated model from this coordinate set for molecular dynamics simulations. A homology model of NR2D was constructed from the NR2A structure, and the hydrated version of this model was subjected to molecular dynamics at 300 K. Modeling of the NR2A and NR2D agonist binding domains demonstrate that despite the overall similarity between the subtypes, structural differences exist that may play important roles in the distinct pharmacological phenotypes. The average structure from the molecular dynamics simulations suggest that the Domain2 of NR2D shows the largest displacement from NR2A. Although most atomic contacts with the ligand are maintained between NR2A and NR2D, we found that NR2D Tyr732 (Tyr711 in NR2A) can switch its interactions. Tyr711 forms an important interdomain hydrogen bond in NR2A in both our model and the NR2A crystal structure, which shifts to an agonist contact for the analogous residue (Tyr732) in NR2D.

Small changes in the ligand orientation, how it interacts with the binding site, and subtle differences in the contacts between the two domains contribute to alteration of the relative positioning of the ligand binding core Domain2. For example, simulations predict that the carbon backbone of glutamate adopts a different orientation in NR2A compared with NR2D. This implies that substituents on agonists for NR2D are placed in a different position than in NR2A. It likewise creates opportunities for the development of subtype-selective agonists or antagonists. SYM2081 (discussed above), which shows a 46-fold increase in potency at NR2D receptors, is one example of a molecule that apparently exploits the different position of the ligand to place a substituent in a position that is favorable in NR2D but not NR2A.

In addition to changes among the contact residues for glutamate in the pocket, there is also an increase in the number of interdomain hydrogen-bonded contacts between the upper and lower domains. Recent structural and functional studies of α-amino-3-hydroxy-5-methyl-4-isoxazolepropionic acid and kainate receptors have raised the idea that interdomain contacts can stabilize the cleft-closed conformation and thus both enhance agonist affinity and slow deactivation time course (Robert et al., 2005; Weston et al., 2006; Hansen et al., 2007). Our data are consistent with these observations. We find that the NR2D subunit, at which glutamate has a higher potency than NR2A, has more interdomain contacts than NR2A. Moreover, mutagenesis studies show that interruption of these interdomain contacts can decrease potency, suggesting that they do provide some stabilization of the closed-cleft conformation, which we interpret to be necessary for channel activation.

Acknowledgments

We thank Antoine Almonte and Kimberly Haustein for excellent technical assistance, and Drs. Hiro Furukawa and Eric Gouaux for sharing unpublished data. M.T.G. and J.P.S. are grateful to Prof. Dennis Liotta (Emory University, Atlanta, GA) for support and encouragement, and Dr. Jamal Musaev and the Emerson Center for Scientific Computation for computational resources and assistance.

References

Anson LC, Chen PE, Wyllie DJA, Colquhoun D, and Schoepfer R (1998) Identification of amino acid residues of the NR2A subunit that control glutamate potency in recombinant NR1/NR2A NMDA receptors. *J Neurosci* **18:**581–589.

Anson LC, Schoepfer R, Colquhoun D, and Wyllie DJA (2000) Single-channel analysis of a NMDA receptor possessing a mutation in the region of the glutamate binding site. *J Physiol* **527:**225–237.

Benveniste M and Mayer ML (1991) Structure-activity analysis of binding kinetics for NMDA receptor competitive antagonists: the influence of conformational restriction. *Br J Pharmacol* **104:**207–221.

Berendsen HJC, Postma JPM, van Gunsteren WF, DiNola A, and Haak JR (1984) Molecular dynamics with coupling to an external bath. *J Chem Phys* **81:**3684–3690.

Berendsen HJC, van der Spoel D, and van Drunen R (1995) GROMACS: A message-passing parallel molecular dynamics implementation. *Comp Phys Comm* **91:**43–56.

Bleakman D (1999) Kainate receptor pharmacology and physiology. *Cell Mol Life Sci* **56:**558–566.

Borza I and Domany G (2006) NR2B selective NMDA antagonists: the evolution of the ifenprodil-type pharmacophore. *Curr Top Med Chem* **6:**687–695.

Buller AL and Monaghan DT (1997) Pharmacological heterogeneity of NMDA receptors: characterization of NR1a/NR2D heteromers expressed in *Xenopus* oocytes. *Eur J Pharmacol* **320:**87–94.

Cali P and Begtrup M, (2002) Synthesis of 1-hydroxypyrazole glycine derivatives. *Tetrahedron* **58:**1595–1605.

Chazot PL (2004) The NMDA receptor NR2B subunit: a valid therapeutic target for multiple CNS pathologies. *Curr Med Chem* **11:**389–396.

Chen PE, Geballe MT, Stansfeld P, Johnston AR, Yuan H, Jacob AL, Synder JP, Traynelis SF, and Wyllie DJA (2005) Structural features of the glutamate binding site in recombinant NR1/NR2A N-methyl-D-aspartate receptors determined by site-directed mutagenesis and molecular modeling. *Mol Pharmacol* **67:**1470–1484.

Chen PE, Johnston AR, Mok MH, Schoepfer R and Wyllie DJ (2004) Influence of a threonine residue in the S2 ligand binding domain in determining agonist potency and deactivation rate of recombinant NR1a/NR2D NMDA receptors. *J Physiol* **558** (Pt 1):45–58.

Chen PE and Wyllie DJA (2006) Pharmacological insights obtained from structure-function studies of ionotropic glutamate receptors. *Br J Pharmacol* **147:**839–853.

Clausen RP, Hansen KB, Cali P, Nielsen B, Greenwood JR, Begtrup M, Egebjerg J, and Bräuner-Osborne H (2004) The respective N-hydroxypyrazole analogues of the classical glutamate receptor ligands ibotenic acid and (*RS*)-2-amino-2-(3-hydroxy-5-methyl-4-isoxazolyl)acetic acid. *Eur J Pharmacol* **499:**35–44.

Colquhoun D (1998) Binding, gating, affinity and efficacy: The interpretation of

structure-activity relationships for agonists and of the effects of mutating receptors. *Br J Pharmacol* **125:**924–947.
Curras MC and Dingledine R (1992) Selectivity of amino acid transmitters acting at *N*-methyl-D-aspartate and amino-3-hydroxy-5-methyl-4-isoxazolepropionate receptors. *Mol Pharmacol* **41:**520–526.
Darkwa J, Mundoma C, and Simoyi RH (1998) Antioxidant chemistry - Reactivity and oxidation of DL-cysteine by some common oxidants. *J Chem Soc, Faraday Trans* **94:**1971–1978.
Dingledine R, Borges K, Bowie D, and Traynelis SF (1999) The glutamate receptor ion channels. *Pharmacol Rev* **51:**7–61.
Do KQ, Herrling PL, Streit P, and Cuenod M (1988) Release of neuroactive substances: homocysteic acid as an endogenous agonist of the NMDA receptor. *J Neural Transmission* **72:**185–190.
Do KQ, Mattenberger M, Streit P, and Cuenod M (1986) In vitro release of endogenous excitatory sulfur-containing amino acids from various rat brain regions. *J Neurochem* **46:**779–786.
Erreger K, Chen PE, Wyllie DJ, and Traynelis SF (2004) Glutamate receptor gating. *Crit Rev Neurobiol* **16:**187–224.
Essman U, Perera L, Berkowitz ML, Darden T, Lee H, and Pedersen LG (1995) A smooth particle mesh Ewald method. *J Chem Phys* **103:**8577–8593.
Furukawa H and Gouaux E (2003) Mechanisms of activation, inhibition and specificity: crystal structures of the NMDA receptor NR1 ligand-binding core. *EMBO J* **22** (12):2873–2885.
Furukawa H, Singh SK, Mancusso R, and Gouaux E (2005) Subunit arrangement and function in NMDA receptors. *Nature* **438** (7065):185–192.
Grieve A, Butcher SP, and Griffiths R (1992) Synaptosomal plasma membrane transport of excitatory sulphur amino acid transmitter candidates: kinetic characterization and analysis of carrier specificity. *J Neurosci Res* **32:**60–68.
Hansen KB, Clausen RP, Bjerrum EJ, Bechmann C, Greenwood JR, Christensen C, Kristensen JL, Egebjerg J, and Bräuner-Osborne H (2005) Tweaking agonist efficacy at N-methyl-D-aspartate receptors by site-directed mutagenesis. *Mol Pharmacol* **68:**1510–1523.
Hansen KB, Yuan H and Traynelis SF (2007) Structural aspects of AMPA receptor activation, desensitization and deactivation. *Curr Opin Neurobiol* **17:**281–288.
Heresco-Levy U, and Javitt DC (1998) The role of N-methyl-D-aspartate (NMDA) receptor-mediated neurotransmission in the pathophysiology and therapeutics of psychiatric syndromes. *Eur Neuropsychopharmacol* **8:**141–152.
Humphrey W, Dalke A, and Schulten K (1996) VMD - visual molecular dynamics. *J Mol Graphics* **14:**33–38.
Jane DE, Olverman HJ, and Watkins JC (1994) Agonists and competitive antagonists: structure-activity and molecular modelling studies, in *The NMDA Receptor* (Collingridge GL and Watkins JC, eds) 2nd ed, pp 31–104, Oxford University Press, Oxford.
Jones KS, VanDongen HM, and VanDongen AM (2002) The NMDA receptor M3 segment is a conserved transduction element coupling ligand binding to channel opening. *J Neurosci* **22:**2044–2053.
Laskowski RA, MacArthur MW, Moss DS, and Thornton JM (1993) PROCHECK: a program to check the stereochemical quality of protein structures. *J Appl Cryst* **26:**283–291.
Layton ME, Kelly MJ 3rd, and Rodzinak KJ (2006) Recent advances in the development of NR2B subtype-selective NMDA receptor antagonists. *Curr Top Med Chem* **6:**697–709.
Lehmann A, Hagberg H, Orwar O, and Sandberg M (1993) Cysteine sulphinate and cysteate: mediators of cysteine toxicity in the neonatal rat brain? *Eur J Neurosci* **5:**1398–1412.
Lindahl E, Hess B, and van der Spoel D (2001) GROMACS 3.0: A package for molecular simulation and trajectory analysis. *J Mol Mod* **7:**306–317.
MacDonald AW 3rd and Chafee MV (2006) Translational and developmental perspective on N-methyl-D-aspartate synaptic deficits in schizophrenia. *Dev Psychopathol* **18:**853–876.
Maier W, Schemm R, Grewer C, and Laube B (2007) Disruption of inter-domain interactions in the glutamate binding pocket affects differentially agonist affinity and efficacy of N-methyl-D-aspartate receptor activation. *J Biol Chem* **282:**1863–1872.
Malenka RC and Nicoll RA (1993) NMDA-receptor-dependent synaptic plasticity: multiple forms and mechanisms. *Trends Neurosci* **16:**521–527.
Mares P, Folbergrova J, and Kubova H (2004) Excitatory aminoacids and epileptic seizures in immature brain. *Physiol Res* **53:**S115–S124.
Mayer ML and Armstrong N (2004) Structure and function of glutamate receptor ion channels. *Annu Rev Physiol* **66:**161–181.
Mayer ML and Westbrook GL (1987) The physiology of excitatory amino acids in the vertebrate central nervous system. *Prog Neurobiol* **28:**197–276.
Monyer H, Burnashev N, Laurie DJ, Sakmann B, and Seeburg PH (1994) Developmental and regional expression in the rat brain and functional properties of four NMDA receptors. *Neuron* **12:**529–540.
Patneau DK and Mayer ML (1990) Structure-activity relationships for amino acid transmitter candidates acting at *N*-methyl-D-aspartate and quisqualate receptors. *J Neurosci* **10:**2385–2399.
Robert A, Armstrong N, Gouaux E, and Howe JR (2005) AMPA receptor binding cleft mutations that alter affinity, efficacy, and recovery from desensitization. *J Neurosci* **25:**3752–3762.
Traynelis SF, Burgess MF, Zheng F, Lyuboslavsky P, and Powers JL (1998) Control of voltage-independent zinc inhibition of NMDA receptors by the NR1 subunit. *J Neurosci* **18:**6163–6175.
Verdoorn TA and Dingledine R (1988) Excitatory amino acid receptors expressed in *Xenopus* oocytes: agonist pharmacology. *Mol Pharmacol* **34:**298–307.
Vicini S, Wang JF, Li JH, Zhu WJ, Wang YH, Luo JH, Wolfe BB, and Grayson DR (1998) Functional and pharmacological differences between recombinant *N*-methyl-D-aspartate receptors. *J Neurophysiol* **79:**555–566.
Wang CX and Shuaib A (2005) NMDA/NR2B selective antagonists in the treatment of ischemic brain injury. *Curr Drug Targets CNS Neurol Disord* **4:**143–151.
Weston MC, Gertler C, Mayer ML, and Rosenmund C (2006) Interdomain interactions in AMPA and kainate receptors regulate affinity for glutamate. *J Neurosci* **26:**7650–7658.
Wriggers W and Schulten K (1997) Protein domain movements: detection of rigid domains and visualization of hinges in comparisons of atomic coordinates. *Proteins* **29:**1–14.
Wyllie DJ, Béhé P, and Colquhoun D (1998) Single-channel activations and concentration jumps: comparison of recombinant NR1a/NR2A and NR1a/NR2D NMDA receptors. *J Physiol* **510:**1–18.
Wyllie DJA, Johnston AR, Lipscombe D, and Chen PE (2006) Single-channel analysis of a point mutation of a conserved serine residue in the S2 ligand binding domain of the NR2A NMDA receptor. *J Physiol* **574:**477–489.
Yuan H, Erreger K, Dravid SM, and Traynelis SF (2005) Conserved structural and functional control of *N*-methyl-D-aspartate receptor gating by transmembrane domain M3. *J Biol Chem* **280:**29708–29716.

Address correspondence to: Dr. Stephen F. Traynelis, Department of Pharmacology, Emory University School of Medicine, 5025 Rollins Research Center, 1510 Clifton Road, Atlanta GA 30322-3090. E-mail: strayne@emory.edu